Cell Biology
Neuroscience

Translational regulation enhances distinction of cell types in the nervous system

Reviewed Preprint
v2 • June 14, 2024
Revised by authors

Reviewed Preprint
v1 • September 26, 2023

Toshiharu Ichinose, **Shu Kondo**, **Mai Kanno**, **Yuichi Shichino**, **Mari Mito**, **Shintaro Iwasaki**, **Hiromu Tanimoto**

Frontier Research Institute for Interdisciplinary Sciences, Tohoku University • Graduate School of Life Sciences, Tohoku University • Faculty of Advanced Engineering, Tokyo University of Sciences • RNA Systems Biochemistry Laboratory, RIKEN Cluster for Pioneering Research, Wako, Saitama 351-0198, Japan • Department of Computational Biology and Medical Sciences, Graduate School of Frontier Sciences, The University of Tokyo, Kashiwa, Chiba 277-8561, Japan

Abstract

Multicellular organisms are composed of specialized cell types with distinct proteomes. While recent advances in single-cell transcriptome analyses have revealed differential expression of mRNAs, cellular diversity in translational profiles remains underinvestigated. By performing RNA-seq and Ribo-seq in genetically-defined cells in the *Drosophila* brain, we here revealed substantial posttranscriptional regulations that augment the cell-type distinctions at the level of protein expression. Specifically, we found that translational efficiency of proteins fundamental to neuronal functions, such as ion channels and neurotransmitter receptors, was maintained low in glia, leading to their preferential translation in neurons. Notably, distribution of ribosome footprints on these mRNAs exhibited a remarkable bias towards the 5' leaders in glia. Using transgenic reporter strains, we provide evidence that the small upstream open reading frames (uORFs) in the 5' leader confer selective translational suppression in glia. Overall, these findings underscore the profound impact of translational regulation in shaping the proteomics for cell-type distinction and provide new insights into the molecular mechanisms driving cell-type diversity.

eLife assessment

This **valuable** paper explores the role of translational regulation in the establishment of differential gene expression between neurons and glia in Drosophila. The paper uses Ribo-seq to show extensive variation in the translation efficiency of specific transcripts between neurons and glia. The evidence supporting the model is **solid**, although only one example (that exhibits very strong differential transcriptional expression between one class of neurons and glia) is studied in detail for translation efficiency.

https://doi.org/10.7554/eLife.90713.2.sa2

Introduction

Gene expression is regulated both at the transcription and translation levels (Becker et al., 2018; Casas-Vila et al., 2017; Li et al., 2020; Liu et al., 2016; Schwanhäusser et al., 2011), and its heterogeneity defines the specialized morphologies and functions of cells. The *Drosophila* brain is a well-studied model tissue with a diverse array of cell types, classifiable by morphology, cell lineage, or gene expression (Scheffer et al., 2020; Zeng and Sanes, 2017). Recent advances in single-cell transcriptomics have identified groups of differentially expressed genes and provided an in-depth overview of transcriptional regulations (Croset et al., 2018; Davie et al., 2018; Li et al., 2022). While these inventories provided a powerful way to classify cell types, there have been cases falling short in explaining proteomic or morphological diversity (Lago-Baldaia et al., 2023; Li et al., 2020). Therefore, posttranscriptional regulations play pivotal roles in distinguishing cell-type specific proteomes.

Ribosome profiling or Ribo-seq, which is based on deep-sequencing of mRNA fragments protected by ribosomes from RNase treatment (ribosome footprints), has been a powerful approach to provide a genome-wide snapshot of protein synthesis ('translatome') (Ingolia et al., 2009). Application of this method, combined with transcriptome analysis, revealed multiple layers of translational regulation in cells. For example, this comparison allowed measurements of translational efficiency (TE), which is quantified as the number of ribosome footprints on the coding sequence per mRNA, and discoveries of previously unannotated ORFs (Dunn et al., 2013; Ingolia et al., 2011, 2009; Zhang et al., 2018). While TE profiles have been reported to be variable among dissected animal tissues (Fujii et al., 2017; Wang et al., 2021; Zhang et al., 2018), differences in translational regulations among identified cell types remain unclear.

Applying ribosome profiling to *Drosophila* heads, we here examine the comprehensive landscape of translational profiles between neuronal and glial cells. Due to the size of the fly brain (~0.5 mm) and intricate intercellular adhesions among neurons and glia (Kremer et al., 2017), surgical separation is impractical. We thus biochemically purified ribosome-bound mRNAs through genetic tagging of ribosomes in target cells (Chen and Dickman, 2017; Sapkota et al., 2019; Scheckel et al., 2020; Thomas et al., 2012; You et al., 2021) and further performed Ribo-seq and RNA-seq. By this comparative transcriptome-translatome analyses, we suggest that differential translational programs enhance the distinction of protein synthesis between neuronal and glial cells.

Results

Comparative transcriptome-translatome analyses reveal translational suppression of selective groups of proteins in the fly heads

To gain an overview of the translation status, we first applied conventional Ribo-seq in the whole fly head, and successfully monitored footprint distribution at a single-codon resolution (**Figure 1A**, see 'Materials and Methods' for technical details). The majority (96.2%) of ribosome footprints was mapped onto the annotated coding sequences (CDS), and its distribution displayed a clear 3-nt periodicity, reflecting the codon-wise movement (**Figure 1B**).

To compare transcriptome and translatome, we also performed RNA-seq from the same lysate (**Figure 1A**). As previously reported, the transcript level and the number of ribosome footprints did not always match, suggesting substantial posttranscriptional regulations (R^2 = 0.664; **Figure**

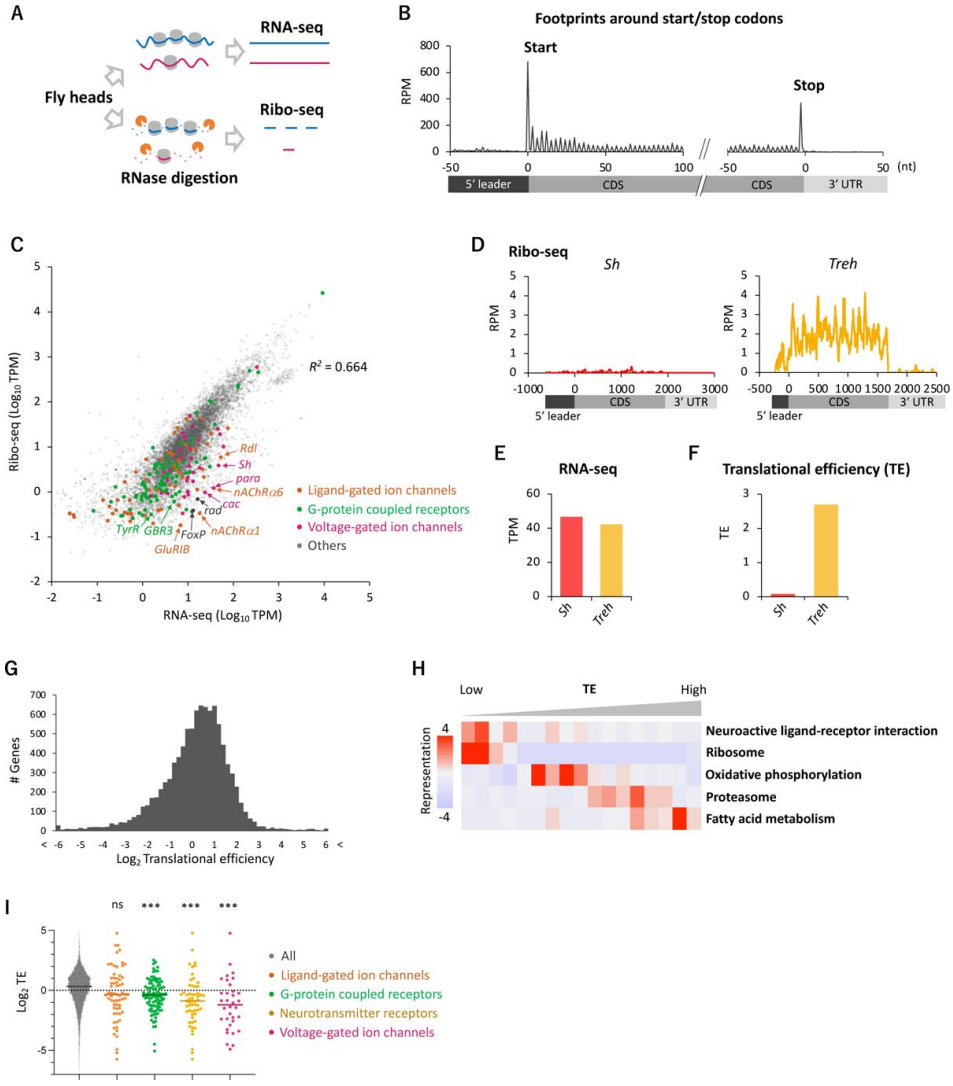

Figure 1.

Comparative transcriptome-translatome analyses in the *Drosophila* head.

(A) Schematics. Fly head lysate is digested with RNase I for Ribo-seq, while not for RNA-seq. Resultant short fragments or the whole mRNA are reverse-transcribed and sequenced. (B) Meta-genome ribosome distribution (estimated P-sites of the 21-nt fragments), relative to the annotated start and stop codons. RPM: reads per million. (C) Scatter plots of mRNA reads (x-axis, TPM: transcripts per million) and ribosome footprints on CDS (y-axis, TPM). Several neuron-related genes are highlighted with colors and arrows. The squared Pearson's correlation coefficient (R^2) is indicated. (D-F) Ribosome footprints (D), mRNA level (E), and translational efficiency (F) of *Shaker-RB* (*Sh*) and *Trehalase-RA* (*Treh*). TE: translational efficiency. TE is calculated as ribosome footprints on CDS (TPM) divided by the mRNA level (TPM). (G) Histogram of TE. The bin size is 0.2 in the unit of log 2. Total 9,611 genes with at least one read in both Ribo-seq and RNA-seq are plotted. (H) Kyoto Encyclopedia of Genes and Genomes (KEGG) pathways enrichment analysis, visualized by iPAGE (Goodarzi et al., 2009), based on TE. The 9,611 genes are ranked and binned according to TE (left to right: low to high), and over- and under-representation is tested. The presented KEGG pathways show *P* values smaller than 0.0005. (I) TE of transcripts in the denoted gene ontology terms. Bars represent the median. ns: $P > 0.05$; ***: $P < 0.001$; in the Dunn's multiple comparisons test, compared to the "all" group.

1C). For instance, while *Shaker* (*Sh*) and *Trehalase* (*Treh*), which encode a voltage-gated K^+ channel and an enzyme that hydrolyzes trehalose, respectively, were similar regarding transcript levels, far more ribosome footprints were detected on *Treh* (**Figure 1D-E**). We therefore measured translational efficiency (TE), ribosome footprints normalized by mRNA reads. TE was much higher for *Treh* than *Sh* (**Figure 1F**), and we found a striking genome-wide variability with more than 20-fold TE difference between the 5 and 95 percentiles (**Figure 1G**). Kyoto Encyclopedia of Genes and Genome (KEGG) pathway enrichment analysis revealed that transcripts involved in fatty acid metabolism and proteasome are actively translated (**Figure 1H**). In contrast, ribosome proteins, as previously reported (Chen and Dickman, 2017; Cho et al., 2015), and proteins mediating neuronal ligand-receptor interactions were significantly enriched in the transcripts with low TE, suggesting translational suppression (**Figure 1H**). Indeed, many transcripts encoding ligand- or voltage-gated ion channels, G-protein coupled receptors (GPCR) showed remarkably low TE (**Figure 1C** and **1I**). These results suggest translational regulations specific to neuronal transcripts in the fly head.

Translational regulation enhances the difference in the gene expression profiles between cell types

Because the translatome/transcriptome status of the whole heads was a mixed average of diverse cell types, such as neurons, glial cells, fat bodies, and muscles, we set up an experimental approach to dissect cell-type specific translational regulations. By expressing epitope-tagged RpL3 (uL3 in universal nomenclature) (Chen and Dickman, 2017) under the control of UAS using the *nSyb*- or the *repo-GAL4* drivers, we immunopurified the tagged ribosomes and associated mRNAs separately from neurons and glia, and performed Ribo-seq (**Figure 2A**). By immunohistochemistry, we confirmed that *UAS-RpL3::FLAG* on the third chromosome exhibited minimum leakage expression in the brain and did not display any apparent morphological defects upon expression using either driver, compared to other insertions or constructs (Chen and Dickman, 2017; Huang et al., 2019; Thomas et al., 2012) (**Figures 2A** and **Figure 2** – figure supplement 1A-B). The exogenously expressed RpL3::FLAG was highly concentrated in cell bodies but also detectable in neurites, consistent with the subcellular localization of the endogenous ribosome (**Figure 2** – figure supplement 1C-D).

Through the purification of FLAG-tagged ribosomes, we successfully profiled translatome from neurons and glial cells in the fly heads: Footprints were found on 10,821 (78.4 % of all the annotated genes) and 10,994 (79.7 %) genes in neurons and glia, respectively, with decent reproducibility among the biological replicates ($R^2 > 0.9$, **Figure 2** – figure supplement 2A). The FLAG-tagged RpL3 in the corresponding cells far exceeded the endogenous RpL3, as RpL3 reads were 7.8 and 42.7 times higher in neurons and glia, respectively, compared to the wild-type whole-head samples (**Figure 2** – figure supplement 2B). The known marker genes were strongly enriched while non-target markers were depleted (**Figures 2B** and **Figure 2** – figure supplement 2C-D) (Croset et al., 2018; Davie et al., 2018; Li et al., 2022), and the KEGG enrichment analysis showed significant enrichment of footprints on genes associated with the known functions of these cell types (**Figure 2** – figure supplement 2E). Interestingly, the KEGG analysis also revealed that neurons exhibit a greater extent of protein synthesis related to oxidative phosphorylation and mitochondrial ribosome proteins, while glial cells show higher expression of proteins associated with glycolysis (**Figure 2** – figure supplement 2E-F). These findings support the glia-neuron lactate shuttle hypothesis, a recently proposed concept of metabolic specialization (Mason, 2017; Volkenhoff et al., 2015). Furthermore, apart from the annotated CDS, we detected clustered ribosome footprints on *Hsr-ω*, previously annotated as a long non-coding RNA, strongly suggesting the synthesis of hitherto undescribed polypeptides (**Figure 2** – figure supplement 2G) (Singh, 2022). Altogether, the combination of genetic labelling of ribosomes in selective cell types and Ribo-seq revealed the differential translatome profiles in the fly heads.

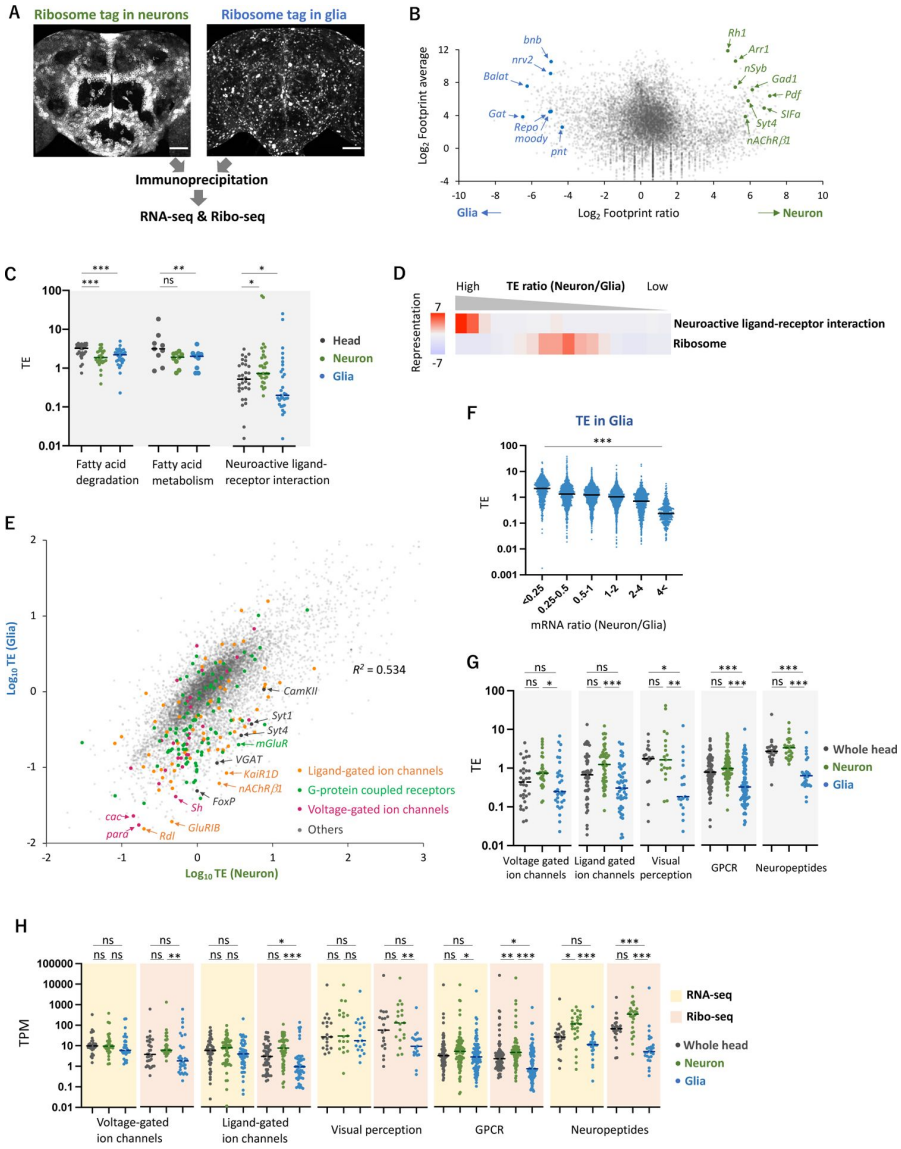

Figure 2.

Cell-type specific Ribo-seq and RNA-seq reveal differential translational regulations.

(A) Schematics. FLAG-tagged ribosome protein L3 (RpL3::FLAG) is expressed in neurons (*nSyb-GAL4*) or in glial cells (*repo-GAL4*). RNA-seq and Ribo-seq are performed following immunoprecipitation. Whole brain images of the exogenously expressed RpL3::FLAG are shown. Scale bars: 50 μm. (B) The MA-plot of ribosome footprints on CDS among neurons and glia. Each gene is plotted according to the fold change (x-axis) and the average (y-axis) in the unit of $\log_2$. Several marker genes are highlighted with green (neuron) or blue (glia). (C) TE of genes in the denoted KEGG pathways in the whole head (black), neurons (green), or in glia (blue). Genes with TPM > 1 in the RNA-seq dataset are plotted. Bars represent the median. *: $P < 0.05$, **: $P < 0.01$, ***: $P < 0.001$, the Dunn's multiple comparisons test. (D) KEGG pathway enrichment analysis based on the ratio of TE in neurons to in glia. All genes with at least one read in both cell types (total 9,732 genes) are ranked and binned according to the neuron-to-glia ratio (left to right: high to low), and over- and under-representation is tested. The presented KEGG pathways show *P* values smaller than 0.0005. (E) Scatter plot of TE in neurons (x-axis) and in glia (y-axis). The squared Pearson's correlation coefficient (R^2) is indicated. (F) TE in glia plotted according to the ratio of mRNA expression in neurons compared to glia. ***: $P < 0.001$, Kruskal-Wallis test. All the 7,933 genes showing TPM > 1 in RNA-seq are analyzed. (G) TE of transcripts, showing at least one read, in the indicated gene ontology (GO) terms. Bars represent the median. **: $P < 0.01$, ***: $P < 0.001$, Dunn's multiple comparisons test. (H) Read counts of genes (TPM) in the indicated GO terms in RNA-seq (yellow) and in Ribo-seq (pink). The grey, green and blue dots indicate the read counts in the whole head, neurons and glial cells, respectively. ns: $P > 0.05$, **: $P < 0.01$, ***: $P < 0.001$, Dunn's multiple comparisons test.

To further examine translational regulation by calculating TE, we performed RNA-seq from the same immunoprecipitated complexes, similar to Translating Ribosome Affinity Purification (TRAP) (Heiman et al., 2008) (**Figures 2A** and **Figure 2** – figure supplement 3A-B). Because this approach relies on the 80S-ribosome-mRNA complex, we may miss mRNA with little or no translation. Nevertheless, our transcriptome was similar to the sn-transcriptome data (Li et al., 2022) (**Figure 2** – figure supplement 3C). We identified groups of genes undergoing neuron- or glia-specific translational regulations compared to the whole heads (**Figure 2** – figure supplement 4A). Genes mediating fatty acid metabolism and degradation, for example, were actively translated in the whole head, but showed lower TE in neurons or in glia (**Figures 1H** and **2C**). Because many of these genes are highly expressed in the fat bodies (Dobson et al., 2018), these results suggest selective translational enhancement in the fat body. Strikingly, TE of genes involved in neuroactive ligand-receptor interaction was significantly higher in neurons but lower in glia (**Figure 2C-D**), suggesting cell-type specific translational regulation of these genes.

This differential translational regulation was highlighted in the weak TE correlation between neurons and glia (R^2 = 0.534, **Figure 2E**). We found a genome-wide tendency that genes transcribed less in glia are further suppressed at translation (**Figure 2F**). Specifically, many functionally-characterized neuronal genes, such as voltage- or ligand-gated ion channels, G-protein coupled receptors, neuropeptides and proteins for visual perception, showed particularly lower TE in glia (**Figures 2E**, 2G-H and **Figure 2** – figure supplement 4C). For these genes, the distinction between neuronal and glial cells was much exaggerated at the level of translation than at transcription (**Figure 2H**). Consistently on the genome-wide scale, the inter-cell type correlation became weaker in Ribo-seq data compared to in RNA-seq (R^2 = 0.59 vs. 0.81, **Figure 2** – figure supplement 3B). Altogether, these data indicate substantial contributions of translational regulation to shaping the cell-type specific protein expression.

Biased distribution of ribosomes toward upstream open reading frames of neural genes in glial cells

We next analyzed the distribution of ribosome footprints on the differentially translated transcripts (DTT). Fat-body related genes showed lower TE in neurons compared to the whole head (**Figure 2C**). Among these genes, we found a remarkable ribosomal accumulation on the start codon specifically in neurons (**Figure 3** – figure supplement 1A-B), as if the first round of the elongation cycle was arrested in neurons. Through the reanalysis of the published RNA-seq data (Dobson et al., 2018), we found that mRNAs showing strong ribosomal accumulation on the start codons are highly abundant in the fat bodies (**Figure 3** – figure supplement 1C). On the other hand, DTTs suppressed in glial cells compared to neurons (defined as genes with more than 10 times higher TE in neurons than in glia, n = 161), we noticed that glial ribosome footprints were remarkably biased towards 5' leaders (**Figure 3A-B**). Notably, this pattern was not obvious on the genome-wide scale (**Figure 3A-B**). The high 5' leader/CDS ratio of ribosome footprints in glia was commonly observed on many transcripts with known neuronal functions, such as *Rab3*, *Syt4*, *Arr1* and *Syn* (**Figure 3D-E**). Conversely, we observed accumulated ribosome footprints on the 5' leaders of several glial marker genes specifically in neurons (**Figure 3** – figure supplement 2). Altogether, these results suggest that the translation of 5' leaders in selective mRNAs differentiates protein synthesis among cell types.

We reasoned translational downregulation via upstream open reading frames (uORFs) in the 5' leaders in glia, as the translation of uORFs was reported to suppress that of the downstream main ORF (Ferreira et al., 2013; Zhang et al., 2019, 2018). Consistent with this idea, metagene plot around the AUG codons on 5' leaders revealed strong accumulation of footprints on the upstream AUG codons, similar to those observed on the initiation codon of CDSs (**Figures 4A-B**). We calculated the footprint accumulation score on each codon (defined as the ratio of footprints on each codon with surrounding −50/+50 nt), and found that upstream AUG and the near cognate codons (NUG or AUN) showed relatively high accumulation (**Figure 4C**). On the other hand,

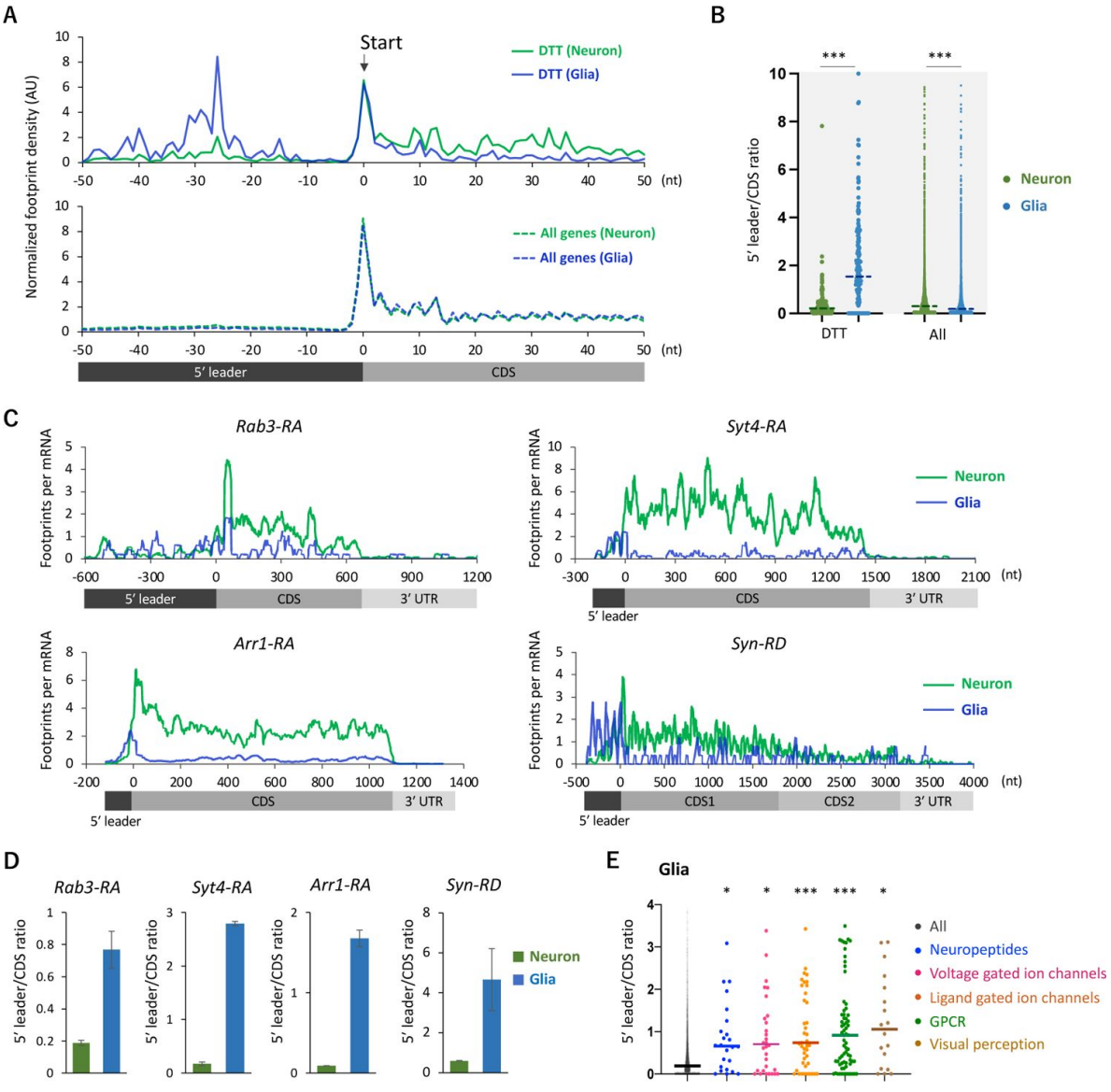

Figure 3.

Ribosome stalling on the 5' leaders of DTTs in glia.

(A) Ribosome distribution (estimated P-sites) on the 161 DTTs around the start codons (solid lines; start +/- 50 nt). These DTTs are defined as transcripts showing more than 10 times higher TE in neurons compared to glia. The dotted lines in the bottom graph indicate the genome-wide distribution. All the transcripts showing TPM > 1 in RNA-seq both in neurons and glia are considered (7,933 genes in total), and the height is normalized by the total reads on this region. (B) Ratio of ribosome density on 5' leader (TPM) to CDS (TPM) of the 161 DTTs or of all transcripts in neurons (green) or in glia (blue). The bars represent the median. ***: $P < 0.001$, Mann-Whitney test of ranks. (C) Distribution of ribosome footprints on the representative neuronal transcripts. Ribosome footprints (RPM) normalized by the mRNA level (TPM) are shown. Note that *Syn-RD* harbors a stop codon in the CDS but a fraction of ribosomes skip it, generating two annotated ORFs (CDS1 and CDS2) (Klagges et al., 1996). (D) Ratio of ribosome density on 5' leader to CDS (mean ± standard error of mean of the biological replicates). (E) Ratio of ribosome density on 5' leader to CDS on transcripts in the indicated GO terms in glia. *: $P < 0.05$, ***: $P < 0.001$, Dunn's multiple comparisons test compared to the "all" group.

inside the annotated CDS, none of the codons exhibited such significant accumulation (**Figures 4D**). Consistently, we found that transcripts related to neuronal functions typically contain long 5' leaders and many upstream AUG (**Figure 4** – figure supplement 1). We thus propose that glial cells suppress the translation of neuronal transcripts by stalling ribosomes on 5' leader via uORF.

uORFs in *Rh1* confer translational suppression in glia

We next asked if the 5' leader sequences of neuronal genes cause cell-type differences in translation. To this end, we focused on *Rh1* (*Rhodopsin 1*, also known as *ninaE*), which encodes an opsin, also detecting stimuli of other sensory modalities (Leung et al., 2020; O'Tousa et al., 1985; Shen et al., 2011; Zuker et al., 1985). Consistently, active translation of Rh1 was almost exclusively observed in neurons (**Figure 5A**). Similar to other neuronal genes shown in **Figure 3C**, the distribution of ribosome footprints was distinct among neuronal and glial cells: they were heavily biased to 5' leader in glia, with the striking accumulation on the putative uORFs composed only of the start and stop codons (**Figure 5B-C**).

To address the function of these sequences on differential traslation, we constructed a transgenic reporter strain using the *Rh1* UTR sequences under the control of UAS (**Figure 5D**), and directed gene expression ubiquitously using *Tub-GAL4*. While the reporter mRNA was detected both in neuronal and glial cells, the protein levels were much more heterogeneous and strikingly weak in glia (**Figure 5E**; **Figure 5** – figure supplement 1A). The control reporter strain (DeLuca and Spradling, 2018), on the other hand, exhibited more ubiquitous expression, with significantly higher fluorescent intensity in glia (**Figure 5E-F**). Driving the reporter expression using the *nSyb-* or *repo-GAL4* further corroborated cell-type specific suppression in glia (**Figure 5** – figure supplement 1B-C). Strikingly, when the 6-base putative uORFs were mutated, the in-vivo protein-to-mRNA ratio of the reporter was significantly increased in glia but not in neurons (**Figure 5G-H**). Based on these results, we propose that glial cells selectively suppress the protein synthesis of neuronal genes through uORF and thereby enhance the translatome distinction from neurons.

Discussion

In this study, the comparative translatome-transcriptome analyses in the whole heads, neurons and glial cells revealed the significant diversity of translational regulations across different cell types. Particularly noteworthy was the differential translation of transcripts encoding neuronal proteins, including ion channels and neurotransmitter receptors (**Figure 2**). These neuronal transcripts exhibited preferential translation in neurons (**Figure 2**), and the relatively long 5' UTR of these transcripts strongly stalled ribosomes in glia (**Figures 3**, 4 and **Figure 4** – figure supplement 1). This characteristic feature of long 5' leaders containing numerous uORFs is also observed in neuronal transcripts in mammals (Glock et al., 2021). While the 5' leader-mediated translational regulations are known to be critical for quick response to environmental changes, such as starvation or oxidative stress (Harding et al., 2003; Mueller and Hinnebusch, 1986; Young and Wek, 2016), our study sheds light on its roles in contrasting protein expression among cell types. Furthermore, considering a pivotal role of *de novo* protein synthesis for long-lasting adaptation (Flexner et al., 1963; Tully et al., 1994), it is plausible that similar mechanisms are employed for neuronal plasticity as well.

The next obvious question would be how the translation of neuronal transcripts is differentiated among neuronal and glial cells. Ribosomes can initiate translation at uORFs more frequently in glia. Alternatively, the post-termination 40S subunits reinitiate translation of the coding sequence more often in neurons. These two possibilities can be distinguished by profiling the rates of initiation or reinitiation, achievable through sequencing the footprints of the 40S subunits, known as translation complex profile sequencing, coupled with conventional Ribo-seq (Archer et al.,

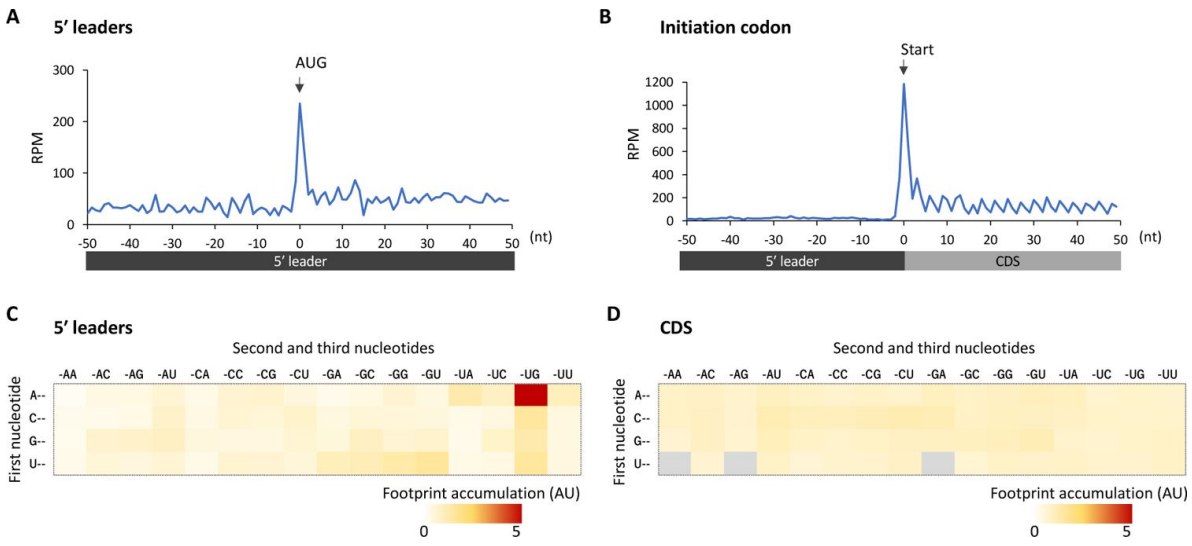

Figure 4.

Footprint accumulation on upstream AUG in glia.

(A) Meta-genome ribosome distribution (estimated P-sites of the 32-nt fragments) around the upstream AUG codons in glia. (B) Meta-genome ribosome distribution (estimated P-sites of the 32-nt fragments) around the annotated start codons in glia. (C) Footprint accumulation on 5' leader in glia, defined as the number of ribosome footprints (estimated P-sites) on each codon normalized by the average on the surrounding (−50 to +50) regions. (D) Footprint accumulation inside the annotated CDS in glia. Annotated in-frame codons except the start and the stop codons are considered. AU: arbitrary unit.

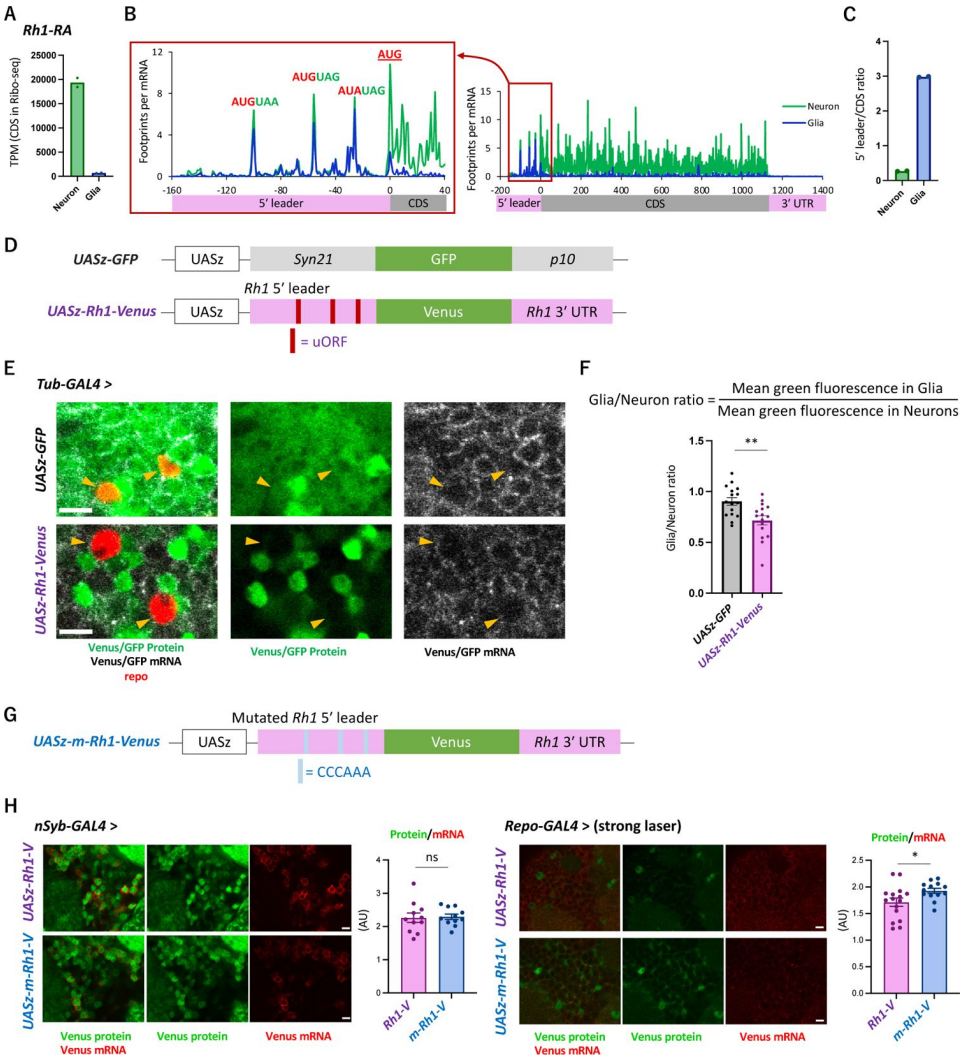

Figure 5.

The transgenic *Rh1-Venus* reporter reveals differential translation in neuronal and glial cells.

(A) Reads on CDS of *Rh1-RA* in Ribo-seq. (B) Ribosome distribution (estimated P-sites) on *Rh1-RA* in neurons (green) and in glia (blue), with 0 on the x-axis indicating the start codon of the CDS. 6-base upstream ORFs, consisting of consecutive start (or the near-cognate) and stop codons, are highlighted. Note that footprints are normalized by the mRNA level (TPM). (C) Ratio of ribosome density on 5' leader (TPM) to CDS (TPM) in neurons (green) or in glia (blue). The bars and the dots represent the median and individual data points, respectively. (D) Schematics of the control (*UASz-GFP*) or the *Rh1* (*UASz-Rh1-Venus*) reporter. For the *Rh1* reporter, 5' leader and 3' UTR sequences of *Rh1-RA* are fused to CDS of the *Venus* fluorescent protein. For the control reporter, synthetic 5' leader sequences (*syn21*) and viral *p10* terminator are fused to GFP (DeLuca and Spradling, 2018). Note that both reporters contain the same promoter (*UASz*) (DeLuca and Spradling, 2018) and are inserted onto the identical genomic locus (*attP40*). (E) Expression of the *Rh1*- or the control reporters driven by *Tubulin-GAL4*. Sliced confocal images of the cortical regions next to the antennal lobe are shown. Green: EGFP or Venus fluorescent signal. Red: Immunohistochemical signal of repo protein as a glial marker. Grey: EGFP or Venus mRNA. Orange arrowheads indicate glial cells marked by the repo expression. Scale bars: 5 μm. (F) Quantification of the green fluorescent intensity in glial nuclei, nomalized by the fluorescence in neurons. Glial intensity was measured as mean intensity in the repo-positive pixels, and was normalized by the mean intensity in the repo-negative pixels. **: $P < 0.01$, Mann-Whitney test of ranks. (G) Schematics of the mutated *Rh1* reporter (*m-Rh1*). The minimal uORF is replaced with CCCAAA. (H) The expression of the *Rh1*- or *m-Rh1*- reporters, driven by the *nSyb*- or the *repo*- GAL4. Sliced confocal images of the cortical regions next to the antennal lobe are shown. Green: Venus fluorescent signal. Red: Venus mRNA signal. The total protein signal was normalized by the total mRNA signal for each brain. $N = 8$ (*nSub* > *Rh1*), 8 (*nSyb* > *m-Rh1*), 16 (*repo* > *Rh1*), 13 (*repo* > *m-Rh1*). ns: $P > 0.05$, *: $P < 0.05$, Mann-Whitney test of ranks.

2016; Bohlen et al., 2020; Wagner et al., 2020). Although there are various technical challenges, the application of this technique to specific cells within the brain would elucidate these possibilities. Furthermore, previous studies have identified eIF1, eIF2α kinases, and DENR/MCT1, as facilitators of translation of main ORF whose 5' leaders harbor uORFs (Ivanov et al., 2010; Schleich et al., 2014; Sonenberg and Hinnebusch, 2009; Zhou et al., 2020). Interestingly, all these proteins are expressed more in neurons than in glia in our dataset (supplementary table 1). Selective activation of these molecular machineries might underlie the cell type specific translation.

Our cell-type specific translatome analysis further revealed translational regulations beyond 5' leaders. We found a remarkable ribosomal stall at the initiation codon in several transcripts, a phenomenon observed in neurons but not in the entire heads (**Figure 3** – figure supplement 1). These transcripts are known to be massively expressed in the fat bodies but less in the nervous system (**Figure 3** – figure supplement 1C) (Dobson et al., 2018), and the translation was further suppressed in neurons (**Figure 3** – figure supplement 1). Therefore, transition from initiation to elongation may serve as another regulatory checkpoint of protein synthesis (Harnett et al., 2022; Wang et al., 2019), which enhances cell-type distinctions. Furthermore, we found ribosome footprints also on the 3' UTR of certain transcripts, such as *Synapsin* (**Figure 3C**). Stop-codon readthrough has been reported to be more frequent in neurons than in other cell types (Hudson et al., 2021; Karki et al., 2022; Prieto-Godino et al., 2016). Because the readthrough events extend the protein C-terminus, its regulation can add yet another layer of cell-type diversity (Dunn et al., 2013; Jungreis et al., 2011; Klagges et al., 1996). Altogether, we here propose that translational regulations further differentiate transcriptome distinctions, thereby shaping the cellular identity.

Due to the specialized functions of neuronal and glial cells, they express distinct sets of proteins. Neurons allocate more ribosomes to proteins related to neurotransmission, visual sensing and oxidative phosphorylation, while glial cells synthesize transporters and enzymes for metabolism of amino acid, fatty acid or carbohydrates (**Figure 2** – figure supplement 1F). Despite these clear differences and specialization, a significant amount of neuronal and glial cells has a common developmental origin. They originate from a stem cell lineage known as neuro-glioblasts (Lai and Lee, 2006; Viktorin et al., 2011), and the fate of these cells can be altered by the expression of a single gene, *glial cells missing* (*gcm*) (Hartenstein, 2011; Hosoya et al., 1995). Therefore, translational regulations, in addition to transcriptional diversity, may play a particularly important role in these sister cell types with distinct physiological roles.

In the *Drosophila* brain, approximately 100 stem cell lineages diverge into more than 5,000 morphologically distinct cell types (Ito et al., 2013; Scheffer et al., 2020; Yu et al., 2013). Hence, translational regulations similar to those described in this study, or other possible regulations, may play significant roles in further differentiating neuronal or glial subtypes. Consistent with this idea, our *UAS-Rh1-Venus* reporter showed heterogeneous expression even among neurons, contrasting with the more uniform expression observed in the control *UASz-GFP* reporter (**Figures 5E** and **Figure 5** – figure supplement 1B-C). In accordance, choline acetyltransferase (ChAT), an enzyme needed to synthesize acetylcholine, and vesicular acetylcholine transporter (VAChT) are transcribed in many glutamatergic and GABAergic neurons but its protein synthesis is inhibited (Chen et al., 2023; Lacin et al., 2019). Substantial post-transcriptional regulations are also implicated during development (Li et al., 2020; Zhang et al., 2016). Taken together, multiple layers of transcriptional and posttranscriptional regulations should shape the proteome diversity of cell types in the nervous system. Further comparative transcriptome-translatome analyses using more specific GAL4 drivers should highlight the diversity of translational regulations leveraged in the brain.

Limitation of the study

Because our cell-type specific Ribo-seq and RNA-seq are based on immunoprecipitation of genetically tagged RpL3 (Chen et al., 2017), the read counts could contain biases, such as underestimation of mRNA level with little or no translational activity, or over- and under-representation of certain cell types originating from the heterogeneous expression of the drivers.

Materials and Methods

Fly culture and genetics

The flies were reared in a mass culture at 24 °C under the 12-12 hour light-dark cycles on the standard cornmeal food. The *Canton-S* strain was used as the wild-type. We utilized the following transgenic strains: w^{1118}*;;GMR57C10-GAL4* (*nSyb-GAL4*; BDSC #39171), w^{1118}*;;repo-GAL4* (BDSC #7415), y^1w^{1118}*;;tublin-GAL4* (BDSC #5138), w^{1118}*;MB010B* (BDSC #68293), w^{1118}*;;UAS-RpL3::FLAG* (BDSC #77132) (Chen and Dickman, 2017), y^1v^1*;UAS-Rh1-Venus* (made in this study; see below), y^1v^1*;UAS-m-Rh1-Venus* (made in this study), *w;UASz-GFP* (a kind gift from Dr. Steven DeLuca) (DeLuca and Spradling, 2018). Females of the GAL4 drivers were crossed to males of the UAS effectors, and the F1 progenies were used for the experiments. Of note, although *UAS-EGFP::RpL10Ab* (Thomas et al., 2012) has been used to isolate ribosomes from specific cells, its expression using the *repo-GAL4* caused lethality in our hands.

Library preparation for ribosome profiling

Tissue collection and lysate preparation

Four to eight days old flies with mixed gender were flash-frozen with liquid nitrogen, thoroughly vortexed, and the heads were isolated from the bodies with metal mesh in a similar manner reported previously (Sun et al., 2020). Approximately 500 frozen heads were mixed with 400 µl of frozen droplets of lysis buffer [20 mM Tris-HCl pH7.5, 150mM NaCl, 5 mM $MgCl_2$, 1 mM dithiothreitol, 1 % Triton X-100, 100 µg/ml chloramphenicol, and 100 µg/ml cycloheximide] in a pre-chilled container, then pulverized with grinding at 3,000 rpm for 15 seconds using a Multi-beads Shocker (YASUI KIKAI). Cycloheximide and chroramphenicol were added to the lysis buffer to prevent possible elongation and run-off of cytosolic and mitochondrial ribosomes, respectively. The lysate was slowly thawed at 4 °C and the supernatant was recovered after spinning down by a table top micro centrifuge. The lysate was treated with 10 U of Turbo DNase (ThermoFisher Scientific) on ice for 10 min to digest the genome DNA. The supernatant was further clarified by spinning at 20,000 g for 10 minutes.

Immunoprecipitation

Anti-FLAG M2 antibody (F1804, Sigma Aldrich) and Dynabeads M-280 bound to anti-mouse IgG antibody (11201D, Invitrogen) were used for immunoprecipitation. 25 µl of the beads solution, washed twice with the aforementioned lysis buffer, was mixed with 2.5 µl of the M2 antibody, and incubated at 4 °C for 1 hour with rotation. Beads were incubated with the lysate at 4 °C for 1 hour with rotation and washed for four times with the lysis buffer. The ribosome-bound mRNA was eluted with 50 µl of 100 µg/ml 3× FLAG peptide (GEN-3XFLAG-25, Protein Ark) dissolved in the lysis buffer.

RNase digestion and library preparation

Ribosome profiling was performed as described previously (McGlincy and Ingolia, 2017; Mito et al., 2020) with modifications. We used RNase I from *E. coli* (N6901K, Epicentre) to digest the crude (**Figures 1**, **Figure 2** – figure supplement 1C-D) or the immunoprecipitated (**Figure 2**) lysate. Concentration of RNA in lysate was measured with Qubit RNA HS kit (Q32852, Thermo Fisher Scientific). RNase I was added at a dose of 0.25 U per 1 µg RNA in a 50 µl reaction mixture, which was incubated at 25 °C for 45 minutes. We used 1.36 µg and 0.5 µg RNA to prepare the whole head libraries (**Figures 1**, **Figure 2** – figure supplement 1C-D) and the cell-type specific libraries (**Figure 2**-**3**), respectively. The RNase digestion was stopped by adding 20 U of SUPERase•In (AM2694, ThermoFisher Scientific). Ribosomes were isolated by MicroSpin S-400 HR columns (27-5140-01, GE Healthcare). Subsequently, we purified RNA using the TRIzol-LS (10296010, ThermoFisher Scientific) and Direct-zol RNA Microprep kit (R2062, Zymo Research), and isolated the RNA fragment ranging 17 to 34 nt by polyacrylamide gel electrophoresis.

The isolated RNA fragments were ligated to custom-made preadenylated linkers containing unique molecular identifiers and barcodes for library pooling, using T4 RNA ligase 2, truncated KQ (M0373L, New England Biolabs) (Mito et al., 2020). Ribosomal RNA was depleted by hybridizing to the custom-made biotinylated 2'-*O*-methyl oligonucleotides with complementary sequences to the *Drosophila* rRNA (see *Supplementary Method* for the sequences), which can be pulled-down using the streptavidin-coated beads (65001, ThermoFisher Scientific). The rRNA-depleted samples were reverse-transcribed with ProtoScript II (M0368L, New England Biolabs), circularized with CircLigase II (CL9025K, Epicentre), and PCR-amplified using Phusion polymerase (M0530S, New England Biolabs) (Mito et al., 2020). The libraries were sequenced with the Illumina HiSeq 4000 system (Illumina) with single-end reads of 50 bases.

Library preparation for transcriptome analysis

The crude (**Figure 1**) or the immunoprecipitated (**Figure 2**) lysate was prepared using the same protocol as described above, but without RNase digestion. RNA was purified using TRIzol-LS. The libraries were constructed in Azenta Japan Corporation, using the NEBNext Poly(A) mRNA Magnetic Isolation Module (E7760, New England Biolabs) and MGIEasy RNA Directional Library Prep kit (1000006386, MGI tech). Briefly, poly-A tailed mRNAs were enriched with the oligo dT beads, fragmented, and reverse-transcribed using random primers. After the second strand cDNA was synthesized, an adapter sequence was added. DNA library was PCR-amplified. The libraries were sequenced with DNB-seq (MGI tech) with an option of paired end reads for 150 bases.

Data analysis

Adaptor sequences were removed using Fastp (Chen et al., 2018), and the reads that matched to the non-coding RNA were discarded. The remaining reads were mapped onto the *Drosophila melanogaster* release 6 genome. Mapping was performed using STAR (Dobin et al., 2013). PCR-duplicated reads were removed by referring to the unique molecular identifiers. The number of uniquely mapped reads are as follows:

Ribo-seq:

Sample	#Reads
Canton-S, whole heads	1,427,090
nSyb-GAL4/UAS-RpL3::FLAG, after IP, replicate 1	2,443,467
nSyb-GAL4/UAS-RpL3::FLAG, after IP, replicate 2	1,135,284
repo-GAL4/UAS-RpL3::FLAG, after IP, replicate 1	2,698,259
repo-GAL4/UAS-RpL3::FLAG, after IP, replicate 2	2,133,920
nSyb-GAL4/UAS-RpL3::FLAG, whole heads, replicate 1	2,147,092
nSyb-GAL4/UAS-RpL3::FLAG, whole heads, replicate 2	2,361,588
repo-GAL4/UAS-RpL3::FLAG, whole heads, replicate 1	1,372,502
repo-GAL4/UAS-RpL3::FLAG, whole heads, replicate 2	1,846,122

RNA-seq:

Sample	#Reads
Canton-S, whole heads	29,132,939
nSyb-GAL4/UAS-RpL3::FLAG, after IP, replicate 1	40,638,850
nSyb-GAL4/UAS-RpL3::FLAG, after IP, replicate 2	34,247,848
repo-GAL4/UAS-RpL3::FLAG, after IP, replicate 1	30,906,375
repo-GAL4/UAS-RpL3::FLAG, after IP, replicate 2	31,928,337

For Ribo-seq analysis, fragments ranging from 20 to 34 nt for whole head samples and 21 to 36 nt for immunoprecipitated samples were used. For the whole head samples, the position of the P site was estimated as 12 or 13 nt downstream from the 5' end, for the 20 to 31 nt or 32-34 nt fragments, respectively (Ingolia et al., 2009). For the immunoprecipitated samples, it was estimated as 12 or 13 nt downstream for the 21 nt or 22-36 nt fragments, respectively. Footprints were considered to be on the CDS if the estimated P site was between the annotated start and stop codons. RNA-seq analysis included all fragments greater than 30 nt in length. For genes with alternatively spliced transcripts, the isoform with the highest TPM in the wild type RNA-seq sample (**Figure 1**) was selected as the 'representative' isoform. If not specified, only the representative isoforms were considered. TE was calculated as TPM of ribosome footprints on CDS divided by TPM of RNA-seq.

The KEGG-enrichment analyses were performed using iPAGE (**Figures 1H** and **2D**) (Goodarzi et al., 2009) or DAVID (**Figure 2** – figure supplement 2E and **Figure 2** – figure supplement 4A) (Dennis et al., 2003). Statistical tests were performed with GraphPad Prism 9.

For the Fly Cell Atlas data (**Figure 2** – figure supplement 3C), expression level was calculated as the mean RPKM in all cells annotated as neuronal or glial cells in heads (Li et al., 2022).

Reporter construct and the transgenic strain

DNA fragments containing a minimal hsp70 promoter (hsp70Bb) (DeLuca and Spradling, 2018), the 5' leader or the mutated 5' leader of *Rh1-RA*, the first 15 bases of the CDS of *Rh1-RA*, the Venus yellow fluorescent protein gene, and the 3' UTR of *Rh1-RA* were synthesized and cloned into the pBFv-UAS3 plasmid (Addgene #138399). The sequence of the resultant plasmid is provided in the *Supporting Information Text*. The plasmid was then injected into y^1 v^1 *P{nos-phiC31}; P{CaryP}attP40*, and their progenies were screened for a *v*+ phenotype. A single transformant was crossed to y^1 cho^2 v^1*; Sp/CyO* balancer to establish a transgenic line.

Immunohistochemistry and fluorescent in-situ hybridization

Immunohistochemistry (**Figures 2A** and **Figure 2** – figure supplement 1) was performed as previously described with minor modifications (Kanno et al., 2021). Briefly, dissected male fly brains were fixed in 2 % paraformaldehyde in PBS for 1 hour at room temperature, washed three times with PBST (0.1 % Triton X-100 in PBS), blocked with 3 % goat serum in PBST for 30 minutes, then incubated with the primary antibody solution at 4 °C overnight (mouse anti-FLAG (1:1000; Sigma-Aldrich; F1804), mouse anti-RpS6 (1:200; Cell Signaling; 54D2), and rat anti-elav (1:20; DSHB; 7E8A10)). Subsequently, the brains were washed three times with PBST, incubated with the secondary antibody solution at 4 °C overnight (anti-mouse Alexa Fluor 488 (1:400; Invitrogen; A11001), anti-mouse Cy3 (1:1000; Jackson ImmunoResearch; 115-166-003), and anti-rat Cy3 (1:200; Jackson ImmunoResearch; 112-166-003)), washed three times with PBST and mounted with 86 % glycerol in PBS.

Fluorescent in-situ hybridization, combined with immunohistochemistry, was performed in a similar manner to (Yang et al., 2017) with several modifications (**Figure 5E-H**). Dissected male fly brains were fixed in PBS containing 3 % formaldehyde, 1 % glyoxal and 0.1 % methanol for 30 min at room temperature, followed by three quick washes with PBT (0.5 % Triton X-100 in PBS). Consistent with the previous study, the addition of glyoxal to the fixative improved the FISH signal (Yao et al., 2021). The buffer was then exchanged to the wash solution (10 % Hi-Di^{TM} Formamide (Thermofisher scientific; 4311320) in 2x saline sodium citrate (SSC)) and was incubated at 37 °C for 5 minutes. Subsequently, the brains were incubated with the custom-made Stellaris *Venus* or *GFP* probes (100 nM; see *Supporting Information Text* for the sequences; LGC BioSearch Technologies) and the primary antibody (mouse anti-Repo (1:100; DSHB; 8D12)) in the hybridization buffer (10% Hi-Di^{TM} Formamide in hybridization buffer (Stellaris RNA FISH Hybridization Buffer, SMF-HB1-10)) at 37 °C for 16 hours. The probes and the antibody were then removed by washing the samples quickly three times with preheated wash solution at 37 °C, followed by three washes for 10 minutes at room temperature. Blocking was performed with 3 % normal goat serum in PBT for 30 min at room temperature. The secondary antibody (Cy3 goat anti-mouse (1:2000; Jackson ImmunoResearch; 115-166-003)) was then added and was incubated at 4 °C overnight. The samples were washed once quickly, three times for 20 minutes, and once for 60 minutes with PBT, and then mounted in 86 % glycerol in 1x Tris-HCl buffer (pH7.4).

Tissues to detect native GFP or Venus signals (**Figure 5** – figure supplement 1) were prepared as follows: dissected brains were fixed in PBS containing 3 % formaldehyde, 1 % glyoxal and 0.1 % methanol for 30 min at room temperature, followed by one quick wash and three washes for 10 minutes with PBT. The samples were then mounted in 86 % glycerol in 1x Tris-HCl buffer (pH7.4).

Imaging and microscopes

Imaging was done on the Olympus FV1200 confocal microscope with GaAsP sensors. A 100x/1.35 silicone immersion objective (UPLSAPO100XS, Olympus) or 30x/1.05 silicone immersion objective (UPLSAPO30XS) was used. Scan settings were kept constant across specimens to be compared.

Data availability

The raw sequence data were deposited in the National Center for Biotechnology Information (NCBI) database with the project code (PRJNA992629). The custom scripts are available in Zenodo (*https://zenodo.org/records/10637789*).

Acknowledgements

We thank Dr. Steven DeLuca (Brandeis University), Dr. Atsushi Sugie (Niigata University), and Dr. Yohei Nitta (Niigata University) for kindly providing the transgenic flies. We also thank Dr. Yusuke Kimura and Dr. Yukihide Tomari (The University of Tokyo) for designing the fly rRNA-depletion probes, Dr. Jasper Janssens (ETH Zurich), Dr. Hongjie Li (Baylor College of Medicine), Dr. Gert Hulselmans (KU Leuven) and Dr. Stein Aerts (KU Leuven) for technical advice regarding analysis of the Fly Cell Atlas data, Ayako Abe (Tohoku University) for technical assistance, Dr. Takashi Makino (Tohoku University) for critical discussion, Madoka Ichinose for critical comments on the graphic design, and the HOKUSAI SailingShip supercomputer facility at RIKEN for computational supports.

This study was supported by the Ministry of Education, Culture, Sports, Science and Technology (MEXT): 21K06369 (to TI), 21H05713 (to TI), JP20H05784 (to SI), JP21K15023 (to YS), 22H05481 (to HT), 22KK0106 (to HT), 20H00519 (to HT); Japan Society for the Promotion of Science (JSPS): 21K06369 (to TI), JP21K15023 (to YS); Japan Agency for Medical Research and Development (AMED): JP23gm1410001 (to SI); Takeda Life Science Research Grant (to TI); RIKEN-Tohoku Univ Science & Technology Hub Collaborative Research Program (to TI and YS), “Biology of Intracellular Environments” (to SI), Special Postdoctoral Researchers (to YS), and Incentive Research Projects (to YS), Tohoku University Research Program “Frontier Research in Duo” (to HT).

References

Archer S.K., Shirokikh N.E., Beilharz T.H., Preiss T (2016) **Dynamics of ribosome scanning and recycling revealed by translation complex profiling** *Nature* **535**:570–574 https://doi.org/10.1038/nature18647

Becker K., Bluhm A., Casas-Vila N., Dinges N., Dejung M., Sayols S., Kreutz C., Roignant J.-Y., Butter F., Legewie S (2018) **Quantifying post-transcriptional regulation in the development of Drosophila melanogaster** *Nat Commun* **9** https://doi.org/10.1038/s41467-018-07455-9

Bohlen J., Fenzl K., Kramer G., Bukau B., Teleman A.A (2020) **Selective 40S Footprinting Reveals Cap-Tethered Ribosome Scanning in Human Cells** *Molecular Cell* **79**:561–574 https://doi.org/10.1016/j.molcel.2020.06.005

Casas-Vila N., Bluhm A., Sayols S., Dinges N., Dejung M., Altenhein T., Kappei D., Altenhein B., Roignant J.-Y., Butter F (2017) **The developmental proteome of Drosophila melanogaster** *Genome Res* **27**:1273–1285 https://doi.org/10.1101/gr.213694.116

Chen N., Zhang Y., Rivera-Rodriguez E.J., Yu A.D., Hobin M., Rosbash M., Griffith L.C (2023) **Widespread posttranscriptional regulation of cotransmission** *Sci. Adv* **9** https://doi.org/10.1126/sciadv.adg9836

Chen S., Zhou Y., Chen Y., Gu J (2018) **. fastp: an ultra-fast all-in-one FASTQ preprocessor** *Bioinformatics* **34**:i884–i890 https://doi.org/10.1093/bioinformatics/bty560

Chen X., Dickman D (2017) **Development of a tissue-specific ribosome profiling approach in Drosophila enables genome-wide evaluation of translational adaptations** *PLoS Genet* **13** https://doi.org/10.1371/journal.pgen.1007117

Cho J. *et al.* (2015) **Multiple repressive mechanisms in the hippocampus during memory formation** *Science* **350**:82–87 https://doi.org/10.1126/science.aac7368

Croset V., Treiber C.D., Waddell S (2018) **Cellular diversity in the Drosophila midbrain revealed by single-cell transcriptomics** *eLife* **7** https://doi.org/10.7554/eLife.34550

Davie K. *et al.* (2018) **A Single-Cell Transcriptome Atlas of the Aging Drosophila Brain** *Cell* **174**:982–998 https://doi.org/10.1016/j.cell.2018.05.057

DeLuca S.Z., Spradling A.C (2018) **Efficient Expression of Genes in the Drosophila Germline Using a UAS Promoter Free of Interference by Hsp70 piRNAs** *Genetics* **209**:381–387 https://doi.org/10.1534/genetics.118.300874

Dennis G., Sherman B.T., Hosack D.A., Yang J., Gao W., Lane H.C., Lempicki R.A. (2003) **DAVID: Database for Annotation, Visualization, and Integrated Discovery** *Genome Biol* **4** https://doi.org/10.1186/gb-2003-4-9-r60

Dobin A., Davis C.A., Schlesinger F., Drenkow J., Zaleski C., Jha S., Batut P., Chaisson M., Gingeras T.R (2013) **STAR: ultrafast universal RNA-seq aligner** *Bioinformatics* **29**:15–21 https://doi.org/10.1093/bioinformatics/bts635

Dobson A.J., He X., Blanc E., Bolukbasi E., Feseha Y., Yang M., Piper M.D.W (2018) **Tissue-specific transcriptome profiling of Drosophila reveals roles for GATA transcription factors in longevity by dietary restriction** . *npj Aging Mech Dis* **4** https://doi.org/10.1038/s41514-018-0024-4

Dunn J.G., Foo C.K., Belletier N.G., Gavis E.R., Weissman J.S (2013) **Ribosome profiling reveals pervasive and regulated stop codon readthrough in Drosophila melanogaster** *eLife* **2** https://doi.org/10.7554/eLife.01179

Ferreira J.P., Overton K.W., Wang C.L (2013) **Tuning gene expression with synthetic upstream open reading frames** *Proc. Natl. Acad. Sci. U.S.A* **110**:11284–11289 https://doi.org/10.1073/pnas.1305590110

Flexner J.B., Flexner L.B., Stellar E (1963) **Memory in mice as affected by intracerebral puromycin** *Science* **141**:57–59 https://doi.org/10.1126/science.141.3575.57

Fujii K., Shi Z., Zhulyn O., Denans N., Barna M (2017) **Pervasive translational regulation of the cell signalling circuitry underlies mammalian development** *Nat Commun* **8** https://doi.org/10.1038/ncomms14443

Glock C., Biever A., Tushev G., Nassim-Assir B., Kao A., Bartnik I., tom Dieck S., Schuman E.M. (2021) **The translatome of neuronal cell bodies, dendrites, and axons** *Proc. Natl. Acad. Sci. U.S.A* **118** https://doi.org/10.1073/pnas.2113929118

Goodarzi H., Elemento O., Tavazoie S (2009) **Revealing Global Regulatory Perturbations across Human Cancers** *Molecular Cell* **36**:900–911 https://doi.org/10.1016/j.molcel.2009.11.016

Harding H.P. *et al.* (2003) **An Integrated Stress Response Regulates Amino Acid Metabolism and Resistance to Oxidative Stress** *Molecular Cell* **11**:619–633 https://doi.org/10.1016/S1097-2765(03)00105-9

Harnett D. *et al.* (2022) **A critical period of translational control during brain development at codon resolution** *Nat Struct Mol Biol* **29**:1277–1290 https://doi.org/10.1038/s41594-022-00882-9

Hartenstein V (2011) **Morphological diversity and development of glia in Drosophila** *Glia* **59**:1237–1252 https://doi.org/10.1002/glia.21162

Heiman M. *et al.* (2008) **A Translational Profiling Approach for the Molecular Characterization of CNS Cell Types** *Cell* **135**:738–748 https://doi.org/10.1016/j.cell.2008.10.028

Hosoya T., Takizawa K., Nitta K., Hotta Y (1995) **Glial cells missing: A binary switch between neuronal and glial determination in drosophila** *Cell* **82**:1025–1036 https://doi.org/10.1016/0092-8674(95)90281-3

Huang K., Chen W., Zhu F., Li P.W.-L., Kapahi P., Bai H (2019) **RiboTag translatomic profiling of Drosophila oenocytes under aging and induced oxidative stress** *BMC Genomics* **20** https://doi.org/10.1186/s12864-018-5404-4

Hudson A.M., Szabo N.L., Loughran G., Wills N.M., Atkins J.F., Cooley L (2021) **Tissue-specific dynamic codon redefinition in Drosophila** *Proc. Natl. Acad. Sci. U.S.A* **118** https://doi.org/10.1073/pnas.2012793118

Ingolia N.T., Ghaemmaghami S., Newman J.R.S., Weissman J.S (2009) **Genome-wide analysis in vivo of translation with nucleotide resolution using ribosome profiling** *Science* **324**:218–223 https://doi.org/10.1126/science.1168978

Ingolia N.T., Lareau L.F., Weissman J.S (2011) **Ribosome Profiling of Mouse Embryonic Stem Cells Reveals the Complexity and Dynamics of Mammalian Proteomes** *Cell* **147**:789–802 https://doi.org/10.1016/j.cell.2011.10.002

Ito M., Masuda N., Shinomiya K., Endo K., Ito K (2013) **Systematic Analysis of Neural Projections Reveals Clonal Composition of the Drosophila Brain** *Current Biology* **23**:644–655 https://doi.org/10.1016/j.cub.2013.03.015

Ivanov I.P., Loughran G., Sachs M.S., Atkins J.F (2010) **Initiation context modulates autoregulation of eukaryotic translation initiation factor 1 (eIF1)** *Proc. Natl. Acad. Sci. U.S.A* **107**:18056–18060 https://doi.org/10.1073/pnas.1009269107

Jungreis I., Lin M.F., Spokony R., Chan C.S., Negre N., Victorsen A., White K.P., Kellis M (2011) **Evidence of abundant stop codon readthrough in Drosophila and other metazoa** *Genome Res* **21**:2096–2113 https://doi.org/10.1101/gr.119974.110

Kanno M., Hiramatsu S., Kondo S., Tanimoto H., Ichinose T (2021) **Voluntary intake of psychoactive substances is regulated by the dopamine receptor Dop1R1 in Drosophila** *Sci Rep* **11** https://doi.org/10.1038/s41598-021-82813-0

Karki P., Carney T.D., Maracci C., Yatsenko A.S., Shcherbata H.R., Rodnina M.V (2022) **Tissue-specific regulation of translational readthrough tunes functions of the traffic jam transcription factor** *Nucleic Acids Research* **50**:6001–6019 https://doi.org/10.1093/nar/gkab1189

Klagges B.R.E., Heimbeck G., Godenschwege T.A., Hofbauer A., Pflugfelder G.O., Reifegerste R., Reisch D., Schaupp M., Buchner S., Buchner E (1996) **Invertebrate Synapsins: A Single Gene Codes for Several Isoforms in Drosophila** *J. Neurosci* **16**:3154–3165 https://doi.org/10.1523/JNEUROSCI.16-10-03154.1996

Kremer M.C., Jung C., Batelli S., Rubin G.M., Gaul U (2017) **The glia of the adult Drosophila nervous system: Glia Anatomy in Adult Drosophila Nervous System** *Glia* **65**:606–638 https://doi.org/10.1002/glia.23115

Lacin H., Chen H.-M., Long X., Singer R.H., Lee T., Truman J.W (2019) **Neurotransmitter identity is acquired in a lineage-restricted manner in the Drosophila CNS** *eLife* **8** https://doi.org/10.7554/eLife.43701

Lago-Baldaia I., Cooper M., Seroka A., Trivedi C., Powell G.T., Wilson S.W., Ackerman S.D., Fernandes V.M (2023) **A Drosophila glial cell atlas reveals a mismatch between transcriptional and morphological diversity** *PLoS Biol* **21** https://doi.org/10.1371/journal.pbio.3002328

Lai S.-L., Lee T (2006) **Genetic mosaic with dual binary transcriptional systems in Drosophila** *Nat Neurosci* **9**:703–709 https://doi.org/10.1038/nn1681

Leung N.Y., Thakur D.P., Gurav A.S., Kim S.H., Di Pizio A., Niv M.Y., Montell C. (2020) **Functions of Opsins in Drosophila Taste** *Current Biology* **30**:1367–1379 https://doi.org/10.1016/j.cub.2020.01.068

Li H. *et al.* (2022) **Fly Cell Atlas: A single-nucleus transcriptomic atlas of the adult fruit fly** *Science* **375** https://doi.org/10.1126/science.abk2432

Li J. *et al.* (2020) **Cell-Surface Proteomic Profiling in the Fly Brain Uncovers Wiring Regulators** *Cell* **180**:373–386 https://doi.org/10.1016/j.cell.2019.12.029

Liu Y., Beyer A., Aebersold R (2016) **On the Dependency of Cellular Protein Levels on mRNA Abundance** *Cell* **165**:535–550 https://doi.org/10.1016/j.cell.2016.03.014

Mason S (2017) **Lactate Shuttles in Neuroenergetics—Homeostasis, Allostasis and Beyond** *Front. Neurosci* **11** https://doi.org/10.3389/fnins.2017.00043

McGlincy N.J., Ingolia N.T (2017) **Transcriptome-wide measurement of translation by ribosome profiling** *Methods* **126**:112–129 https://doi.org/10.1016/j.ymeth.2017.05.028

Mito M., Mishima Y., Iwasaki S (2020) **Protocol for Disome Profiling to Survey Ribosome Collision in Humans and Zebrafish** *STAR Protocols* **1** https://doi.org/10.1016/j.xpro.2020.100168

Mueller P.P., Hinnebusch A.G (1986) **Multiple upstream AUG codons mediate translational control of GCN4** *Cell* **45**:201–207 https://doi.org/10.1016/0092-8674(86)90384-3

O'Tousa J.E., Baehr W., Martin R.L., Hirsh J., Pak W.L., Applebury M.L (1985) **The Drosophila ninaE gene encodes an opsin** *Cell* **40**:839–850 https://doi.org/10.1016/0092-8674(85)90343-5

Prieto-Godino L.L., Rytz R., Bargeton B., Abuin L., Arguello J.R., Peraro M.D., Benton R (2016) **Olfactory receptor pseudo-pseudogenes** *Nature* **539**:93–97 https://doi.org/10.1038/nature19824

Sapkota D. *et al.* (2019) **Cell-Type-Specific Profiling of Alternative Translation Identifies Regulated Protein Isoform Variation in the Mouse Brain** *Cell Reports* **26**:594–607 https://doi.org/10.1016/j.celrep.2018.12.077

Scheckel C., Imeri M., Schwarz P., Aguzzi A (2020) **Ribosomal profiling during prion disease uncovers progressive translational derangement in glia but not in neurons** *eLife* **9** https://doi.org/10.7554/eLife.62911

Scheffer L.K. *et al.* (2020) **A connectome and analysis of the adult Drosophila central brain** *eLife* **9** https://doi.org/10.7554/eLife.57443

Schleich S. *et al.* (2014) **DENR– MCT-1 promotes translation re-initiation downstream of uORFs to control tissue growth** *Nature* **512**:208–212 https://doi.org/10.1038/nature13401

Schwanhäusser B., Busse D., Li N., Dittmar G., Schuchhardt J., Wolf J., Chen W., Selbach M (2011) **Global quantification of mammalian gene expression control** *Nature* **473**:337–342 https://doi.org/10.1038/nature10098

Shen W.L., Kwon Y., Adegbola A.A., Luo J., Chess A., Montell C (2011) **Function of Rhodopsin in Temperature Discrimination in Drosophila** *Science* **331**:1333–1336 https://doi.org/10.1126/science.1198904

Singh A.K (2022) **Hsrω and Other lncRNAs in Neuronal Functions and Disorders in Drosophila** *Life* **13** https://doi.org/10.3390/life13010017

Sonenberg N., Hinnebusch A.G (2009) **Regulation of Translation Initiation in Eukaryotes: Mechanisms and Biological Targets** *Cell* **136**:731–745 https://doi.org/10.1016/j.cell.2009.01.042

Sun H., Nishioka T., Hiramatsu S., Kondo S., Amano M., Kaibuchi K., Ichinose T., Tanimoto H (2020) **Dopamine Receptor Dop1R2 Stabilizes Appetitive Olfactory Memory through the Raf/MAPK Pathway in Drosophila** *J. Neurosci* **40**:2935–2942 https://doi.org/10.1523/JNEUROSCI.1572-19.2020

Thomas A., Lee P.-J., Dalton J.E., Nomie K.J., Stoica L., Costa-Mattioli M., Chang P., Nuzhdin S., Arbeitman M.N., Dierick H.A (2012) **A Versatile Method for Cell-Specific Profiling of Translated mRNAs in Drosophila** *PLoS ONE* **7** https://doi.org/10.1371/journal.pone.0040276

Tully T., Preat T., Boynton S.C., Del Vecchio M (1994) **Genetic dissection of consolidated memory in Drosophila** *Cell* **79**:35–47 https://doi.org/10.1016/0092-8674(94)90398-0

Viktorin G., Riebli N., Popkova A., Giangrande A., Reichert H (2011) **Multipotent neural stem cells generate glial cells of the central complex through transit amplifying intermediate progenitors in Drosophila brain development** *Developmental Biology* **356**:553–565 https://doi.org/10.1016/j.ydbio.2011.06.013

Volkenhoff A., Weiler A., Letzel M., Stehling M., Klämbt C., Schirmeier S (2015) **Glial Glycolysis Is Essential for Neuronal Survival in Drosophila** *Cell Metabolism* **22**:437–447 https://doi.org/10.1016/j.cmet.2015.07.006

Wagner S., Herrmannová A., Hronová V., Gunišová S., Sen N.D., Hannan R.D., Hinnebusch A.G., Shirokikh N.E., Preiss T., Valášek L.S (2020) **Selective Translation Complex Profiling Reveals Staged Initiation and Co-translational Assembly of Initiation Factor Complexes** *Molecular Cell* **79**:546–560 https://doi.org/10.1016/j.molcel.2020.06.004

Wang H. *et al.* (2021) **Tissue- and stage-specific landscape of the mouse translatome** *Nucleic Acids Research* **49**:6165–6180 https://doi.org/10.1093/nar/gkab482

Wang J., Johnson A.G., Lapointe C.P., Choi J., Prabhakar A., Chen D.-H., Petrov A.N., Puglisi J.D (2019) **eIF5B gates the transition from translation initiation to elongation** *Nature* **573**:605–608 https://doi.org/10.1038/s41586-019-1561-0

Yang L., Titlow J., Ennis D., Smith C., Mitchell J., Young F.L., Waddell S., Ish-Horowicz D., Davis I (2017) **Single molecule fluorescence in situ hybridisation for quantitating post-transcriptional regulation in Drosophila brains** *Methods* **126**:166–176 https://doi.org/10.1016/j.ymeth.2017.06.025

Yao R.-W., Luan P.-F., Chen L.-L (2021) **An optimized fixation method containing glyoxal and paraformaldehyde for imaging nuclear bodies** *RNA* **27**:725–733 https://doi.org/10.1261/rna.078671.120

You S., Yu A.M., Roberts M.A., Joseph I.J., Jackson F.R (2021) **Circadian regulation of the Drosophila astrocyte transcriptome** *PLoS Genet* **17** https://doi.org/10.1371/journal.pgen.1009790

Young S.K., Wek R.C (2016) **Upstream Open Reading Frames Differentially Regulate Gene-specific Translation in the Integrated Stress Response** *Journal of Biological Chemistry* **291**:16927–16935 https://doi.org/10.1074/jbc.R116.733899

Yu H.-H. *et al.* (2013) **Clonal Development and Organization of the Adult Drosophila Central Brain** *Current Biology* **23**:633–643 https://doi.org/10.1016/j.cub.2013.02.057

Zeng H., Sanes J.R (2017) **Neuronal cell-type classification: challenges, opportunities and the path forward** *Nat Rev Neurosci* **18**:530–546 https://doi.org/10.1038/nrn.2017.85

Zhang H., Dou S., He F., Luo J., Wei L., Lu J (2018) **Genome-wide maps of ribosomal occupancy provide insights into adaptive evolution and regulatory roles of uORFs during Drosophila development** *PLoS Biol* **16** https://doi.org/10.1371/journal.pbio.2003903

Zhang H., Wang Y., Lu J (2019) **Function and Evolution of Upstream ORFs in Eukaryotes** *Trends in Biochemical Sciences* **44**:782–794 https://doi.org/10.1016/j.tibs.2019.03.002

Zhang K.X., Tan L., Pellegrini M., Zipursky S.L., McEwen J.M (2016) **Rapid Changes in the Translatome during the Conversion of Growth Cones to Synaptic Terminals** *Cell Reports* **14**:1258–1271 https://doi.org/10.1016/j.celrep.2015.12.102

Zhou F., Zhang H., Kulkarni S.D., Lorsch J.R., Hinnebusch A.G (2020) **eIF1 discriminates against suboptimal initiation sites to prevent excessive uORF translation genome-wide** *RNA* **26**:419–438 https://doi.org/10.1261/rna.073536.119

Zuker C.S., Cowman A.F., Rubin G.M (1985) **Isolation and structure of a rhodopsin gene from D. melanogaster** *Cell* **40**:851–858 https://doi.org/10.1016/0092-8674(85)90344-7

Editors

Reviewer #1 (Public Review):

This study seeks to understand how selective mRNA translation informs cellular identity using the Drosophila brain as a model. Using drivers specific for either neurons or glia, the authors express a tagged large ribosomal subunit protein, which they then use as a handle for isolating total mRNA and ribosome footprints. Throughout the study, they compare these data sets to transcriptional and ribosome profiles from the whole fly head, which contains multiple cell types including fat tissue, pigment cells and others, in addition to neurons and glia. Using GO term analyses, they demonstrate the specificity of their cell-type-based ribosome profiling: known glial mRNAs are efficiently translated in glia and likewise in neurons as well. In further examining their RNAseq data set, they find that "neuronal" mRNAs, such as ion channels, are expressed in both neurons and glia, but are translated at higher rates in neurons. Based on this, they hypothesize that neuronal mRNAs are actively suppressed in glia, and next seek to determine the underlying mechanism. By meta-analysis of all mapped ribosome footprints, they find that glia have higher ribosome occupancies in the 5' leader of neuronal mRNAs. This is corroborated by individual ribosome occupancy profiles for several neuronal mRNAs. In 5'leaders containing upstream AUG codons, they find that the glial data sets show an enrichment of ribosomes at these upstream start sites. They thus conclude that that 5' leaders containing upstream AUGs confer translational suppression in glia.

Overall, the sequencing data sets generated in this study and their subsequent bioinformatic analyses seem robust and reliable. Their data echo the trends of cell-type specific translational profiles seen in previous studies (e.g. 27380875, 30650354), and making their data sets and analyses accessible to the broader scientific community would be quite helpful. The findings are presented in a logical and methodical manner, and the data are depicted clearly. The authors' results that 5' leaders facilitate translation suppression is well-supported in literature. However, they overinterpret their data by claiming that such suppression is key for maintaining glial/neuronal identity (it is even featured in their title), but do not present any evidence that loss of such regulation has any impact on cellular identity. In many places, the authors do not acknowledge possible biases in their analytical methods, or consider alternate explanations for their data. These weaken the manuscript in its current form, but many of these issues which I describe below, are rectifiable with modest effort.

(1) The authors' data in Fig. 2-S1A-B shows substantial cell-to-cell variation in RpL3::FLAG expression. The authors do not consider that this variation may cause certain neuronal/glial types to be overrepresented in their datasets. In related, the authors do not discuss whether

RpL3::FLAG only present in the cell body or if it is also trafficked to the neuronal/glial processes where localized translation is known to occur (reviewed in 31270476).

(2) The RNA-seq data set that they use to calculate translation efficiency (TE) only represents mRNAs associated with RpL3::FLAG, which is part of the large ribosome subunit. As the authors are likely aware, there are mRNAs on which the full ribosome moiety does not assemble and these are effectively excluded from this data set. Ideally, a more complete picture of the mRNA landscape can be obtained by 40S subunit profiling but I appreciate that this is technically very challenging. At minimum, this caveat needs to be acknowledged.

How does the TPM of differentially regulated transcripts (such as those in Fig. 2H) compare between whole heads, neurons and glia? Since the whole head RNA-seq data was not from an enriched sample, this might serve as a decent proxy for showing that the neuron/glia RNA-seq data sets are representative of RNA abundance.

(3) The analysis in Fig. 2F shows that low abundance mRNAs in glia are further translationally suppressed, which the authors point out in lines 151-152. However, this data also shows that mRNAs with a 1:1 ration in neuron:glia (which fall in the 0.5-1 and 1-2 bin) have a TE-1; this suggests that on average, mRNAs that are equally abundant are translated equally efficiently. This is the opposite of the thesis presented in Fig. 2G-H where many mRNAs of equal abundance in neurons and glia are actually poorly translated in glia. How do the authors reconcile these observations?

It is also unclear from the manuscript whether all mRNAs were considered for the analysis in Fig. 2F or if some cutoff was employed.

(4) Throughout the manuscript the authors favor a "translation suppression" model wherein glia (for example) actively suppress neuronal mRNAs, and this is substantiated in Fig. 3C showing higher ribosome occupancy on 5' leaders than in coding regions. However, they show no evidence that glial mRNAs (such as those indicated in Fig. 2B and 2-S2B) present a different pattern, say that of higher ribosome occupancy in CDS vs. 5' leaders. This type of a positive control is a glaring omission from many of their analyses, including ribosome occupancy at upstream AUG codons (Fig. 4).

In related, to make a broad case (as they do in the title) that differential translation regulation specifies multiple cell types, it is necessary to show the corollary: that glial mRNAs (repo, bnb, pnt, etc) are suppressed in neurons. There is an inkling of this evidence in Fig. 3-S1 where fat body mRNAs in neurons are shown to have low ribosome occupancy in the CDS regions and enhanced occupancy in the 5' leader region. This data is not quantified, nor is a control neuron mRNA shown as a reference for what the ribosome occupancy profile of an actively translated mRNA looks like in a neuron.

(5) The cell-type specific ribosome profiling data sets in the manuscript are from mRNAs associated with 80s subunits that have been treated with cycloheximide during sample preparation. Cycloheximide, and many other translation inhibitors, are known to non-uniformly bias reads towards start codons (PMID: 22056041,22927429). This important caveat and its implications on the start-codon occupancy analysis in Fig. 4 are not acknowledged in the manuscript.
Again, the ideal resolution would be ribosome profiling data set from 40S footprinting or harringtonine-treated samples (PMIDs: 32589966, 27487212, 32589964) to show true accumulation of ribosomes at AUG codons. In the absence of such a data set, a comparative meta-analysis of the ribosome distribution around upstream and initiation AUG codons of differentially translated transcripts from neurons would be a useful control.

(6) The authors chose Rhodopsin 1 (Rh1) as a model mRNA which is translated efficiently in neurons but suppressed in glia. Though the data in Fig. 2-S3B shows higher TE for Rh1 in neurons, the data in 5A show lower ribosome occupancy in the Rh1 CDS in neuron samples

(at least in the fragment of the CDS visible). These data are somewhat contradictory. Further, given that the neuron data are from all nsyb-positive cells but that Rh1 is expressed only in R1-R6 photoreceptors, it is unclear what motivated them to chose Rh1 as opposed to an mRNA that is more broadly expressed in neurons.

(7) Similar to the heterogeneity in nsyb- and repo-GAL4 expression in Fig. 2-S1A-B, Fig. 5C shows substantial variation in the expression of the UAS-GFP reporter driven by tub-GAL4. This variable GAL4 activity makes the mRNA abundance data difficult to interpret. Also, since the authors presume that Rh1 mRNA is expressed in glia (it is not annotated in the RNA-seq analysis in Fig. 2-S2B), would Rh1-GAL4 not be a more apt driver?
These issues are further compounded by the lack of a cellular compartment marker (repo marks glial nuclei) which makes it impossible to determine which cell the mRNA signal is in. There are also no negative controls are presented for the mRNA probes.

Most confoundingly though, the control reporter itself seems to show variable translation efficiencies from one cell to another, with high-GFP protein cells showing lower GFP mRNA and vice versa.
The mRNA:protein ratio may be easier to examine by using repo-GAL4 to specifically drive the Rh1-reporter expression in glia (such as in Fig. 5-S1A) rather than simultaneous expression in both neurons and glia using tub-GAL4.

Comments post revision: The authors have satisfactorily addressed most of my concerns with the study. I appreciate their patient clarification of many of my points, and the revision to text+figures appending more controls. My only minor gripe remains that while their data beautifully show that there is differential regulation of transcripts across neurons and glia, they do not provide evidence that such regulation is required for cell identity. However, I appreciate this is a large experimental ask worthy of another study in and of itself. Overall, I peg this an excellent study that adds substantially to the field of cell-type specific mRNA translation regulation.

https://doi.org/10.7554/eLife.90713.2.sa1

Reviewer #3 (Public Review):

It is well established that there is extensive post-transcriptional gene regulation in nervous systems, including the fly brain. For example, dynamic regulation of hundreds of genes during photoreceptor development could only be observed at the level of translated mRNAs, but not the entire transcriptomes. The present study instead addresses the role of differential translational regulation between cell types (or rather classes: neurons and glia, as both are still highly heterogenous groups) in the adult fly brain. By performing bulk RNA-seq and Ribo-seq on the same lysates, the authors are able to compare translation efficiency (TE) of all transcripts between neurons and glia. Many genes display differential TE, but interestingly, they tend to be the genes that already show strong differences at their mRNA level. The most striking observation is the finding that neuronal transcripts in glia display increased ribosome stalling at their 5' UTR, and in particular at the start codons of short "upstream ORFs". This could suggest that glia specifically employ a mechanism to upregulate upstream ORF translation, enabling them to better suppress the expression of the genes that have them. And neuronal genes tend to have longer 5' UTRs, perhaps to facilitate this type of regulation.

However, it is difficult to evaluate the functional significance of these differences because the authors provide only one follow-up experiment to their RNA-seq analysis. Venus expressed with the Rh1 UTR sequences may be displaying differential levels between glia and neurons, but I find this image (Fig. 5C) rather unconvincing to support that conclusion. There are no quantifications of colocalization, or even sample size information provided for this experiment. And if there is indeed a difference, it would still be difficult argue this is because

of the 5' stalling phenomenon authors observe with Rh1, because they switched both the 5' and 3' UTRs.

I also find it puzzling that the TE differences between the groups are mostly among the transcripts that are already strongly differentially expressed at the transcriptional level. The authors would like to frame this as a mechanism of 'contrast sharpening'; but it is unclear why that would be needed. Rh1, for instance, is not just differentially expressed between neurons and glia, but it is actually only expressed by a very specific neuronal type (photoreceptors). Thus it's not clear to me why the glia would need this 5' stalling mechanism to fully suppress Rh1 expression, while all the other neurons can apparently do so without it.

Response to authors' revisions:

The authors have addressed most of the technical points in their revised manuscript. However, it is still rather unclear whether this mechanism would have any significant impact on differential gene expression between cell types in vivo. Considering that it's mostly occurring on genes that are already strongly differentially transcribed, that doesn't appear very likely.

https://doi.org/10.7554/eLife.90713.2.sa0

Author response:

The following is the authors' response to the original reviews.

> ***Reviewer 3:***
>
> *Response to authors' revisions:*
>
> *This reviewer is not convinced that the authors have done enough to satisfactorily address either of the major issues described in the original public review, above.*
>
> *They're still not providing a quantification of Fig. 5D (originally 5C).*
>
> *Their response regarding the expression pattern of Rh1 is particularly concerning, as it represents a misinterpretation of previously published data.*
>
> *The gene encoding Rh1, ninaE, is expressed at such high levels in R1-6 PRs that any RNA-seq data (bulk or single-cell) generated from the optic lobes, no matter what cell-type, will display some ninaE transcripts that are present in the background, as they leak from R1-6 during dissociation steps. This phenomenon has been well described, for instance in Davis et al., 2020, eLife, and in fact led to the development of computational tools to abate such artifacts. In other words: no,* rh1 *is not expressed in glia, or any other neuron besides PRs for that matter. Therefore, I remain deeply suspicious about the functional relevance of the regulatory mechanisms described in this paper.*

We thank the reviewer for her or his critical comments.

We quantified the cell-type differences in translation of the reporter with *Tub-GAL4* and now show the results in Figure 5F. Consistent with other results, this analysis revealed that the glia-to-neuron ratio of the reporter protein expression is significantly lower when it contains the UTR sequences of *rh1*.

We removed the mRNA counts (former Figure 5A and Figure 5 - figure supplement 1A), as we agree that these may well be contaminated by the very high *rh1* expression in R1-6. We also amended the graph showing the ribosome distribution on the *rh1* mRNA (Figure 5B) to better compare the translational efficiency (footprints normalized with mRNA, in a similar manner

to Figure 3C). Now it clearly highlights the cell-type differences of footprint distributions; ribosomes are much more enriched on the CDS (being translated) in neurons, while the fraction of ribosomes on the 5′leader (being stalled) is much higher in glia. We summarized this differential ribosome distribution in a new graph (now Figure 5C).

We apologize for the misleading description of the reporter experiments. Despite the high level of mRNA expression in the R1-6, we chose the 5′leader of *rh1* for the translation reporter, as it contains clear uORFs and differential ribosome accumulation thereon (Figure 5B). This biased ribosome distribution and differential translation are the consistent features for many neuronal genes (Figure 3). We revised the text to clarify this point (Line 195-203).

In summary, we provide more rigorous analysis and extensive revision, which we hope clarified the concern.

https://doi.org/10.7554/eLife.90713.2.sa3